Defense Technical Information Center
Compilation Part Notice

ADP010835

TITLE: Analysis of P-band Synthetic Aperture
Radar for Airborne and Spaceborne Applications

DISTRIBUTION: Approved for public release, distribution unlimited
Availability: Document partially illegible.

This paper is part of the following report:

TITLE: Space-Based Observation Technology

To order the complete compilation report, use: ADA391327

The component part is provided here to allow users access to individually authored sections
of proceedings, annals, symposia, ect. However, the component should be considered within
the context of the overall compilation report and not as a stand-alone technical report.

The following component part numbers comprise the compilation report:
ADP010816 thru ADP010842

Analysis of P–band Synthetic Aperture Radar for Airborne and Spaceborne Applications

[1,2]A. Potsis, [1]N. Uzunoglou, [1]P. Frangos, [2]R. Horn, [2]K. Lamprecht

[1]National Technical University Of Athens. Department Of Electrical And Computer Engineering
9 Iroon Polytexniou Str.GR –15780 Zografos, Athens, Greece

[2]German Aerospace Center (DLR) Institute for Radio Frequency Technology.
D–82230 Oberpfaffenhofen, Germany. Tel/Fax (49)8153–282367/281135

Email: athanasios.potsis@dlr.de, nuzu@cc.ece.ntua.gr, pfrangos@central.ntua.gr, ralf.horn@dlr.de, katja.lamprecht@dlr.de

Summary: An increasing amount of interest has evolved in VHF/UHF SAR applications. These types of radars have proven to be a very powerful method for underground and obscured object detection. In this paper we analyze the possibility of a spaceborne P–band SAR system, based on the experience gained from the analysis of the experimental airborne P–band SAR (E–SAR)system of DLR. We address possible methods and filters for effective Radio Frequency Interference (RFI) suppression, polarimetric and radiometric calibration procedures. We also assess the problems concerning the image quality degradation due to ionospheric propagation effects based on several simulation models.

1. INTRODUCTION

In recent years a new class of Synthetic Aperture Radar (SAR) systems using low frequency have emerged. Behind these developments lie technological advances in antenna design, low noise amplifiers, bandpass filters, digital receiver technology as well as new processing algorithms. The combination of low frequency and high bandwidth, creates a variety of applications. Emerging military and civilian applications of P–Band radar systems include the detection of targets concealed by foliage and / or camouflage, detection of buried objects (like the Unexploded Ordnance (UXO) and underground communication and power lines), forestry applications, biomass measuring, archeological and geological exploration.

The above applications of a P–band SAR system have already been explored and demonstrated using mainly airborne systems [1],[2]. All this variety of applications makes the idea of opening a new low frequency spectral window from space for global coverage very attractive.

However the VHF/UHF portion of the spectrum is heavily used for commercial as well as military purposes. Therefore RF interferences (RFI) are typically encountered in the received radar signals. In most of the cases, the presence of RFI in SAR imagery diminishes the usefulness of the processed data [3],[4],[5]. Additionally, accurate calibration of both amplitude and

phase of quad–polarized SAR data is essential for most of the applications [8]. Especially calibration of quadpolarized SAR data is essential if we are to analyze and understand of what kind polarimetric signatures actually are, if we are to compare low frequency backscattered data between scenes and within scenes, and if we are to compare the observations with theory. These are some of the main problems appearing in an airborne P–band system.

In the spaceborne case, the structure and the composition of the ionosphere is strongly correlated to wave propagation performance. The ionosphere behaves as an anisotropic medium and influences the refraction index, which becomes a function of space and time. This has a strong impact on the propagating wave. Due to the changing refraction and diffraction properties and due to the resulting dispersion relation the ionosphere influences both the propagation path (the direction of the wave vector) and the properties of the propagating wave itself. These problems arising from the propagation effects of the VHF/UHF signal through the ionosphere are additive to the problems addressed in the airborne case [23].

In this paper we analyze the possibility of a spaceborne P–band SAR system, based on the experience gained from the analysis of the experimental airborne P–band SAR system of DLR. We address possible methods and filters for effective RFI suppression, polarimetric and radiometric calibration procedures as well as hardware modifications. We also assess the problems concerning the image quality degradation due to propagation effects through the ionosphere, as well as the possibility that a spaceborne SAR sensor will introduce RFI signals to the terrestrial communication channels.

2. E–SAR P–BAND SYSTEM

The E–SAR is a multi–frequency SAR system mounted on board a Dornier DO–228 aircraft (Figure 1), which is owned and operated by DLR [1]. Currently the radar is operational in the P–, L–, C– and X–Bands with selectable vertical or horizontal antenna polarization. SAR interferometry and SAR polarimetry are functional modes of the radar established in 1996 [2].

The resolution of the E–SAR image products is up to 1.5 m in slant range. Typical swath width are 3 and 5 km and the scene length is not limited in general. For motion compensation purposes the Dornier 228 aircraft is equipped with a CCNS4/ Aerocontrol navigation system coupled with DGPS and INS. This assures the measurement of the platform position with an accuracy of 0.1m rms, and of its attitude by 0.01 degrees. The system also gives the pilot an online control about the actual flight path to help keeping the nominal track with an accuracy better than 5m. This reduces the amount of motion compensation during SAR data processing by one order of magnitude.

Nevertheless, since the E–SAR system is installed on a very unstable platform on low altitudes having long aperture times, a proper processing algorithm with a convenient motion compensation approach, has been developed [2]. For the calculations of the motion compensation phase the imaged terrain is assumed to be flat at some reference level. This assumption is justified for a single–pass acquisition and moderate terrain elevation changes [2], but in the repeat pass a complete and accurate phase evaluation is performed.

E–SAR P–Band System	
Parameter	Typical Value
Center frequency [MHz]	450
Pulse bandwidth [MHz]	18 or 50
Chirp duration [μsec]	5
Sample rate [MHz]	60
Forward velocity [m/s]	80-95
PRF [Hz/channel]	500
Flight altitude [m]	3000-5000
Incidence angle [deg]	25-60
Interferometric mode	Repeat-Pass
Across-track baseline [m]	Variable
Baseline tilt. vert. [deg]	Variable

Table 1. Basic operational parameters of the E–SAR P–band system.

In the last years a big effort has been made for improving the efficiency of the P– Band system (center frequency: 450MHz).

The system has been equipped with a new high power amplifier (HPA) of 53 dB gain and peak power of 200 Watts. Additionally a 60MHz band–pass filter was implemented before the low noise amplifier to avoid signal distribution by out–of–band broadcasting frequencies. The high isolation requirements between the four polarization channels was achieved by the implementation of a new 50 dB PIN switch.

As already mentioned before, in low frequency SAR systems it is very likely to have very strong signals due to the nadir echo as well as the radio frequency interference. These strong signals drive the E–SAR 6 bit ADC's into saturation. In order to accommodate these strong signals the RF receiving path was modified to prevent the saturation of the ADC. According to these modifications most of the effective bits of the ADC were used to sample the low amplitude radar backscattered signals and as less as possible bits for the high amplitude RFI signals.
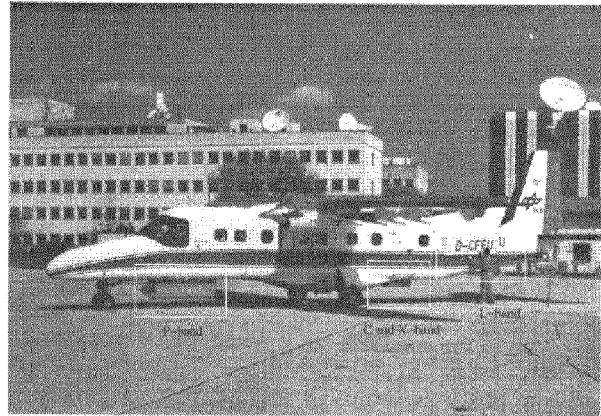

Figure 1. The E–SAR system mounted on a Do–228 aircraft. The antennas of the multi frequency SAR system are depicted in the yellow

The system performance is mainly determined by the antenna which consists of a 2mx4m microstrip ellement array at a center frequency of 450 Mhz. Azimuth beamwidth is 30^0 and elevation one of $\sim60^0$. The basic operating parameters of the E–SAR P–band system are depicted in Table 1. [8]

It the next section, the basic problems that scientists have to face in most of the cases in an airborne VHF/UHF SAR system, namely the presence of RF interferences, the high calibration requirements of interferometric applications and the low Signal–To–Noise ratio (over unvegetated areas), will be briefly discussed and the procedures applied in the E–SAR P–band system in order to overcome these problems will be presented.

3 AIRBORNE P–BAND

3.1 RADIO FREQUENCY INTERFERENCE FILTERING

As already mentioned above, the both requirements of wide bandwidth for high resolution and a low frequency range for foliage or ground penetration necessitate use of frequency bands occupied by other communication channels. As a result, radio frequency interferences (RFI) appear in the receive signal. In most of the cases, the presence of RFI in SAR imagery diminishes the usefulness of the processed data making extremely difficult any attempt for radiometric and polarimetric calibration. In the airborne P–band case we consider interferences coming from other communication sources operating at the same frequency

but for the spaceborne case we will analyze the case where a spaceborne P–band SAR will introduce interferences to the terrestrial communication systems.

E–SAR P–band data contaminated with RFI have been analyzed and several RFI filtering methods have been tested [3],[4],[5]. Two operational RFI suppression filters were the result of this effect.

The first is a very simple and robust frequency domain notch filter which removes the interference peaks by setting a small bandwidth around the detected peaks to zero. This RFI filter is very fast and gives quite acceptable quality data but it has all the disadvantages of a notch filter (sidelobe effects, removing a part of the SAR signal resulting in a degradation of the image quality).

The second RFI suppression filter is based on the least mean square estimation (LMS) algorithm. As described in [3] the algorithm models the RFI signals as a superposition of sinusoidal signals. The general model of the received signal is:

$$X(k)=S(k)+n(k)+\sum_{i=1}^{N} A_i e^{j(2\pi f_i k+\varphi_i)} \tag{1}$$

where X(k) is the received signal, S(k) is the 'pure' target return SAR signal, n(k) is the noise signal (uniformly distributed random variables with zero mean) and the RF interference signals. According to the model (1), every interference signal was detected, estimated and coherently subtracted in each range line in the raw data. This filter provides better quality data than the notch filter as it achieves better signal preservation but it is slower.

The amplitude image and the interferogram of the VV channel of the test site of Gilching/Germany before and after RF interference filtering using the LMS algorithm filter are shown in Figure 2. From this figure becomes evident the "destructive" effect of the RFI signals to the SAR data especially at the interferogram which appears to be completely destroyed, and the filtering improvement.
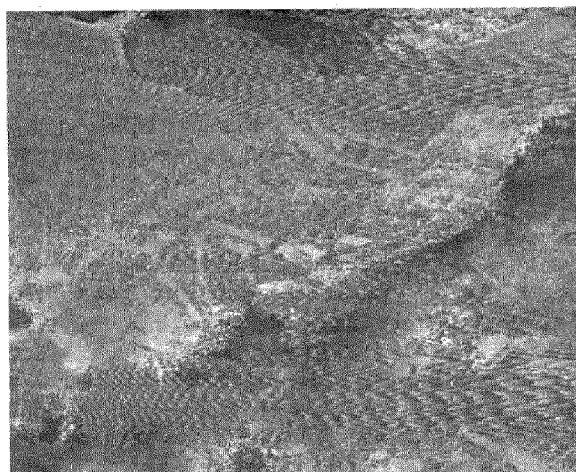
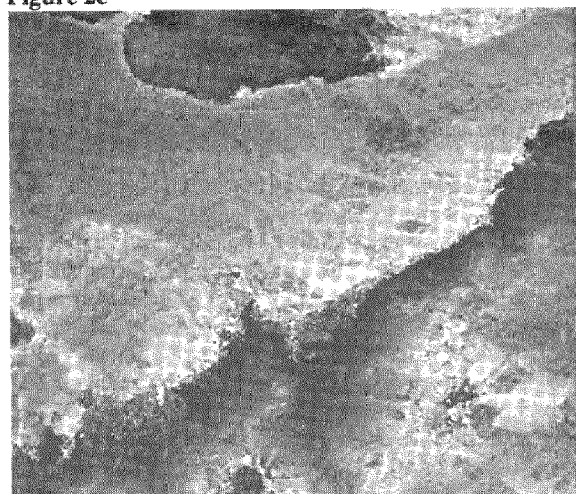

Figure 2a

Figure 2b

Figure 2c

Figure 2d

Figure 2 a. *The unfiltered amplitude image (VV channel) of the test site of Gilching/Germany. The RFI effect it is evident.* **2b.** *The interferogram of the same area (repeat pass interferometric pair with baseline of 40m). The destructive effect of the interference signals to the interferometric phase is here more than evident.* **2c.**

The amplitude image after RFI filtering using the LMS algorithm with resolution in range, 4m and in azimuth, 3m and finally 2d. The interferogram after filtering. The biggest amount of the phase information has been successfully recovered. Near range on the left site of the image. This flight campaign was partially supported by DERA Farnborough UK.

A new mode of operation of the airborne E–SAR system called Listen Only (LO) channel mode of operation, gave us the opportunity to study and analyze the special characteristics of the interfering signals and how they effect the SAR data quality. The basic idea of the LO channel mode of operation is shown in Figure 3. From this Figure becomes evident that in order to be able to store the interfering spectrum between two successive radar pulses we have to implement a control signal [4].
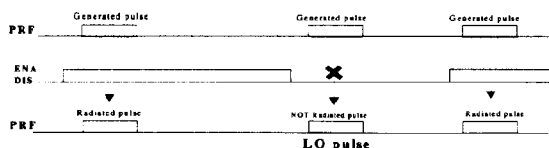

Figure 3: *Basic idea of the LO channel mode of operation.*

When this signal was set to high voltage (Enable–ENA) the generated chirp signal was directed to the antenna for radiation as in the usual operating mode but when this signal was set to low voltage (Disabled –DIS) the generated chirp was not transmitted. The new important information that this mode of operation provides to us, a rises from the fact that the whole spectrum of the interference signals before and after the radar pulse is available. For the first time we have stored the entire interference signal, in all polarizations, and we can analyze how it distorts the backscattered radar signal (amplitude and phase) in the previous and in the next pulse.

Polarimetric analysis of the LO data [4] showed that it is very likely to have interference tones in both polarization states (fully polarimetric) making extremely difficult any attempt to introduce a polarimetric RFI suppression filter. Changes in the polarization state (and probably decorelation effects) of the H polarized RFI signals in successive pulses have also been detected. Statistic analysis showed that the amplitude of the interferences remains almost constant for one range line but it can not be supposed to remain constant for 5 or 10 E–SAR range lines.

A simple notch filter which uses the frequency information of the LO pulse in order to filter the interferences in the next pulse (Radar+RFI) was finally implemented [4]. In general the filter detects in the spectrum the position of the interference (which most of the times appears as high picks) signal and then it sets to zero a small bandwidth of 50kHz at the same position at

the previous radar pulse which contains the back–scattered signal plus the interferences.

There are two main advantages of this filtering approach:

a) This method is very fast and can give filtered data almost in **real time**.

b) All the existing interference signals inside a radar pulse can be detected and successfully removed by the filter regardless of their corresponding amplitude. Without the LO mode it is almost impossible for any estimation algorithm to successfully detect and remove these small amplitude signals in a backscattered data line. This filter was applied on repeat pass interferometric polarimetric data collected by DLR's E–SAR System on the test site of Oberpfaffenhofen /Germany. The filtering results are depicted in Figure 4. From Figure 4 we can see that almost all periodic disturbances generated by interferences have been successfully removed.
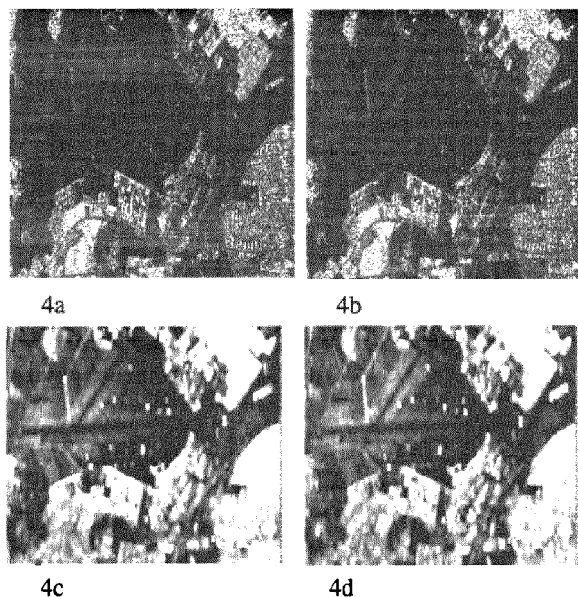

4a   4b

4c   4d

Figure 4: *(a) Unfiltered amplitude image of Ch HH, (b) filtered data with a real time notch filter using interference information from LO Ch. H, (c) unfiltered coherence map of (a) and (d) the filtered coherence map. Near range on the left site of the image.*

The experience gained from the airborne P–band RFI signal analysis, the filtering algorithms that have been already developed and successfully implemented, and especially the idea of the LO channel mode of operation, which can provide almost "real time" interference filtering, can be applied to a spaceborne P–band system ensuring interference free data.

3.2 RADIOMETRIC AND POLARIMETRIC CALIBRATION

As VHF/UHF SAR systems become more and more commonly available to the research community, the radiometric and polarimetric calibration of this kind of

systems becomes important. The high calibration requirements of interferometric applications and P–band characteristic problems as the low Signal–To–Noise ratio (over unvegetated areas) and, as already discussed, the presence of RF interferences make it necessary to adapt, modify, and extend the existing calibration methods, in order to establish a operational calibration [8].

Several calibration flights have been made recently using the modified E–SAR P–band system. The developed calibration procedure and the accuracy that has been achieved are described in this paper. In the next section, the special calibration demands and constraints the scientists have to face in a spaceborne P–band case mainly due to wave propagation effects through the ionosphere, are analytically discussed.

• Calibration of the RFI filtering effect

After the RFI filter has been applied, the total energy of each range line is reduced according to the amount of the subtracted interference signals. This energy reduction is compensated afterwards. In general, the gain of a filter $H(f)$ applied on a stationary (signal) process of power spectral density $A(f)$ is [13]:

$$k_{s,filter} = \frac{\int A(f)|H(f)|^2 df}{\int A(f) df} \qquad (2)$$

This gain $k_{s,filter}$ caused by the LMS filter was calculated and corrected in every filtered range line in the raw data.

• Radiometric calibration.

Adequate radiometric corrections of the P–band E–SAR data require knowledge of the sensor–target geometry and the antenna elevation pattern. Preflight measurements have been performed and the P–band antenna patterns were checked, corrected and stored.

The intensity of the backscattered signal in the raw data and in the processed image can be written as: [8]

$$P = P_s + P_N \ , \quad I = I_s + I_N \qquad (3)$$

Where P_s is the signal intensity in the raw data, P_N is the noise intensity in the raw data, I_s and I_N is the signal intensity and the noise intensity in the image respectively. According to [4], for one homogenous distributed area with "radar brightness" β^0 we get:

$$\bar{I} := \bar{I}_s + \bar{I}_N = K_s \bar{P}_s + K_N \bar{P}_N = K_s C_s \beta^0 + K_N \bar{P}_N \qquad (4)$$

Where,

$$C_s = \frac{c}{2} \frac{\lambda^2}{(4\pi)^3} \frac{\varphi_a E_{TX} G_R G^2(\vartheta - \vartheta_i)}{R^2} \qquad (5)$$

and K_S is the signal gain of the processor for distributed scatterers, K_N is the processor noise gain, λ is the wavelength, φ_a is the effective beam width of the azimuth antenna diagram, E_{TX} is the transmitted chirp energy (=transmit power x chirp duration), G_R is the receiver path gain, $G^2(\vartheta - \vartheta_i)$ is the two way elevation antenna pattern, where ϑ is the off–boresight angle and ϑ_i is the off–nadir look angle, and R is the slant range distance.

To assure that the signal gain remains constant in time and space the following equation must be valid:

$$K_S \propto \frac{1}{C_S} \propto \frac{R^3}{\lambda^2 \varphi_a E_{TX} G_R G^2(\vartheta - \vartheta_i)} \qquad (6)$$

In the processor, using the stored antenna diagrams, all the range and azimuth corrections are applied after range compression using the radiometric calibration function (6).

Several calibration experiments have been made and more than five, three meter trihedral corner reflectors with known RCS value have been used for absolute radiometric calibration. The corner reflectors have been placed in different test sites (Etterschlag and Gilching) and in incidence angles from 25° to 60°. Using the antenna elevation patterns, the corresponding boresight angle and the gain of the system receiving path, radiometrically corrected P band E–SAR data have been analyzed. The data have been processed to an absolute radiometric calibration factor of K_S= 60 dB.

The measured RCS, the signal to background ratio and the measured calibration factor for the two corner reflectors are presented in Table 2.

Track 1	Incidence angle (in deg)	Calibration factor [dB]	Theoretical RCS [dB*sqm]	Estimated RCS [dB*sqm]	signal –to– background ratio [dB]
Polarization state HH					
CR1 (near range)	36.62	61.01	28.75	29.74	25.86
CR2 (far range)	54.27	58.9	28.82	27.73	25.3
Polarization state VV					
CR1 (near range)	36.62	61.7	28.75	30.46	26.52
CR2 (far range)	54.27	58.8	28.82	27.39	26.45

Table 2: *The measured RCS, the signal to background ratio and the measured calibration factor for the two corner reflectors in both polarization states.*

From Table 2 we can conclude that the measured calibration factor is close to the expected one of the 60 dB (less than 1.5 dB variation). Considering the imbalance of the calibration constant, the measured RCS of the corner reflectors appear to be very close to the theoretical value [8],[9],[12]. Using RCS imbalance information from the corner reflector analysis the E–SAR antenna pattern was afterwards corrected.

A second evaluation has been performed concerning the stability from pass to pass. The same test site has been calibrated based on trihedral measurements of the first track. The pass to pass stability is observed to be in

the order of 0.3 dB, meaning that the system shows good temporal stability.[12]

More calibration experiments are planned for the near future. With this experiment we expect to increase our calibration knowledge and to improve even more the performance and the stability of the P–band E–SAR system.

- **Polarimetric calibration**

Qualitative and quantitative evaluation of the scattering matrix data acquired by the airborne E–SAR fully polarimetric P–band system, requires the estimation and elimination of the system induced distortions. This is necessary in order to identify and analyze the underlying scattering matrix.

A large number of polarimetric calibration methods based on different assumptions concerning the system distortion and utilizing backscattering properties of deterministic and distributed scatterers, can be found in the literature [11],[12]. For the polarimetric calibration of the modified P–band system we used the modified Quegan's calibration approach. According to [11], for the airborne SAR case with the absence of the ionospheric effects, the model which describe the systems effects is a two–stage liner distortion model for receive and transmit given by:

$$[O]=[R][S][T]+[N] \qquad (7)$$

where *[O]* is the 2x2 observed scattering matrix, *[S]* is the target scattering matrix, *[R]* and *[T]* are 2x2 complex matrices describing amplitude and phase distortions in the receiver and transmit path respectively and *[N]* is the system noise. The polarimetric calibration consists of the following steps:

i) **Cross–Talk Removal**

In order to accurately estimate the system cross–talk ratios ($w=R_{hv}/R_{vv}$, $u=R_{vh}/R_{hh}$, $z=T_{hv}/T_{hh}$ and $v=T_{vh}/T_{vv}$) two effects had to be taken into account. Firstly the areas which appear to have high correlation between the co- and cross polarized channels (>0.3) [11] have been masked out before the cross–talk estimation. The second effect is the low signal–to–noise ratio (SNR) especially over unvegetated areas which mainly effects the cross polarized channels. These noise affected areas have been excluded and an average $-\alpha-$ range profile for the whole scene was estimated and used for the cross–talk removal. Additionally the range profiles of the estimated cross–talk ratios were used in the correction procedure. Figure 5 depicts the $u=R_{vh}/R_{hh}$ and $v=T_{vh}/T_{vv}$ cross–talk ratios of the data of Figure 2, before and after cross–talk calibration. From this figure we can see that the cross talks can be improved in the order of 13dB resulting values from -33dB and even below -45dB.

ii) **Symmetrisation**

According to [11], symmetrisation of the cross polarised channels based on the least–square solution has been performed.

iii) **Phase Calibration**

The signal response from the trihedral corner reflectors deployed in the test sites in different ranges and incidence angles, with known ratio S_{HH}/S_{VV} was used in order to estimate the complex receive channel imbalance. Evaluation of the collected data showed that after the phase calibration the HH–VV phase imbalance reduces to the order of 10^0 which is, in most of the cases, acceptable for polarimetric applications [12].

iv) **Absolute Inbalance Calibration**

The amplitude imbalance ratio of HH and VV channels was derived from the same trihedral corner reflectors. In order to estimate the energy in both co–polar channels of the cross–talk corrected images the integral method was used [11]. Evaluation of the calibrated data showed that the amplitude imbalance takes values close to 0.1 dB.

The RGB representation of a Pauli [11] decomposition of an RFI filtered, radiometric and polarimetric calibrated E–SAR P–band data of the test site of Gilching / Germany, is depicted in Figure 6.
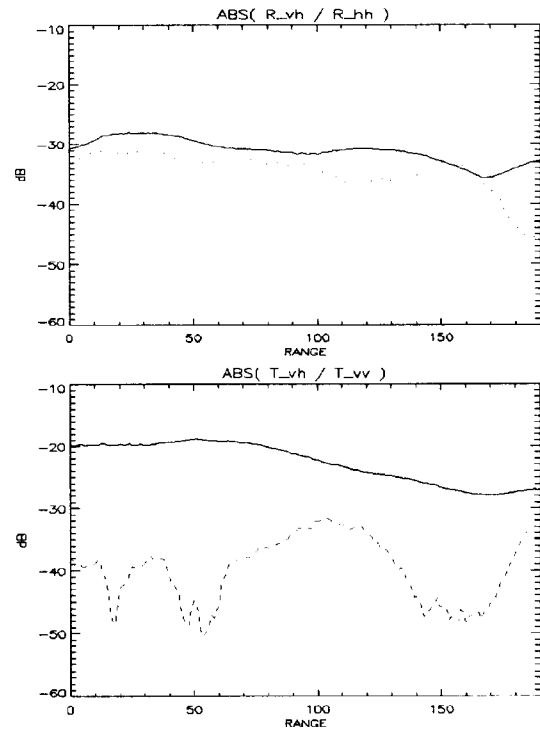

Figure 5: *The estimated cross–talk ratios before (solid lines) and after (dash–dot) the calibration is performed.*

4 SPACEBORNE P–BAND

Scientific fields and the several remote sensing campaigns by the E–SAR P–band system contributed intensively to the development of algorithms and understanding the sensitivity of interferometric fully polarimetric VHF/UHF SAR systems to surface and subsurface detection and parameter estimation. As already presented, the technological progress in

VHF/UHF SAR systems has resulted in the development of new hardware design, signal processing and RFI filtering algorithms, polarimetric and radiometric calibration techniques providing data that are fine tuned for detecting and measuring various Earth surface as well as sub–surface targets and parameters of great interest for the user community (military, forest management, Biomass estimation, archeology etc.).
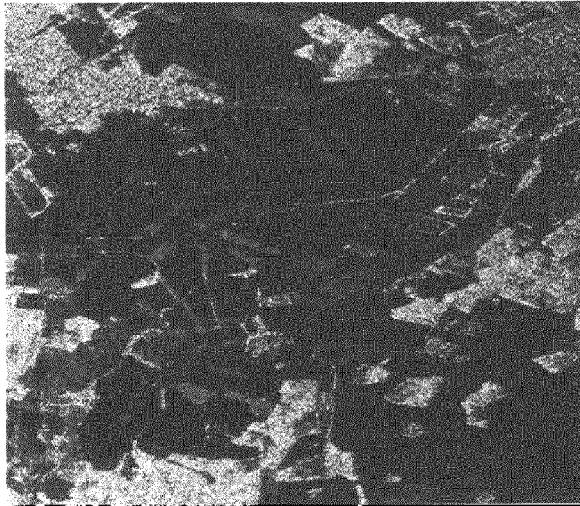

Figure 6: *The RGB representation of a Pauli decomposition of a full polarimetric E–SAR P–band data set of the test area of Gilching/Germany (colors : Red: HH–VV, Green :2HV and Blue: HH+VV.) Near range on the left site of the image. This flight campaign was partially supported by DERA Farnborough UK.*

The wave length used so far for space applications extend to L–band [23],[27],[30]. Adding a new band at longer wavelengths is only meaningful if only sufficient spacing between the wavelengths can be achieved so that the scattering properties of the radar waves become significantly different. The experience gained by operating the E–SAR P–band system with center frequency of 450MHz and 50MHz bandwidth, proved that P–band frequency is adequate as far as the scattering properties are concerned and it is technically feasible on small platforms like the Do–228 airplane. Hence, the frequency band from 400MHz up to 500MHz has been investigated.

But, as all the above variety of applications makes the idea of opening a new low frequency spectral window space for global coverage very attractive, at the same time, it becomes a great challenge for the scientists as the propagation effects of the electromagnetic waves, at VHF/UHF frequency caused by the ionosphere, become significant and can not be ignored.

Irregularities in the propagation medium can cause fluctuations in the phase, amplitude and polarization vector of the radar signal. These errors can be expressed as a sum of two terms, the first a mean value across the synthetic aperture, and the second a fluctuating component [15]. Especially the second one can cause severe distortions of the signal causing difficulties for

any attempt not only for radiometric and polarimetric calibration but also for the data processing itself.

The main parameters in a VHF/UHF SAR scenario which are affected by ionospheric propagation are the azimuth and range resolution, the image position and the orientation angle of the incoming polarized wave [15],[23],[24]. Additional problems in such a system design are the RFI introduced to the radar by the terrestrial communication systems and vice versa, as well as the frequency allocation problem. These problems as well as possible solutions will be analyzed in this section.

4.1 IONOSPHERIC EFFECTS

• **Azimuth resolution**

According to [23], the fluctuations of the refractive index and thus phase fluctuations of the signal due to the ionoshperic turbulences affect the coherence length of the wave field. Depending on the value of the Total Electron Density (TEC) and the used frequency, it might be reduced below the equivalent aperture size D/2, as it happens for P–band frequencies, and thus the azimuthal resolution becomes larger than the half of the antenna aperture size (D/2).

According to [23], the azimuthal resolution of a spaceborne P–band system is very sensitive to the frequency. Changing for example the center frequency from 400MHz to 500MHz we can expect great improvement in the resulting azimuth resolution.

• **Total Electron Density (TEC)**

The Total Electron Density (TEC) is defined as the integration of the electron density over the vertical path from the ground to the upper ionosphere [17]. The value of the TEC changes with solar activities, and the differences can be found with a factor of 3.

The correct and as accurate as possible estimation of TEC variations is essential for the compensation of the ionospheric effects in the radar signal. Different methods have been already used, like satellites and high–altitude rockets, to estimate TEC. An important contribution to the ionosphere TEC mapping has the worldwide network of the Global Positioning System (GPS) [22],[18],[19]. According to [18], the accuracy of the generated TEC maps are restricted, beside hardware errors, by multipath of signal propagation at low elevation, by the limited amount of ground receiving station and by the used model for mapping slant TEC values to vertical values, like assuming a shell ionosphere with constant peak hight [21], [18]. Special care has to be taken in using vertical TEC values of given TEC–references for slant path analysis. By measuring the GPS phase fluctuations, that means by measuring the time rate of differential phase of the dual frequency GPS signals, this network–based system enables to monitor the generation and the changes of the ionospheric irregularities continuously around the globe under various geophysical conditions. As described in [16] instead of measuring the TEC

values, several theoretical models can be applied and the TEC values can be estimated. The more accurate and detailed this knowledge is, the better we can estimate the appropriate time for remote sensing applications [20].

• Range resolution

The dispersion and to a lesser extend the multiple scattering due to ionospheric turbulence result in a pulse broadering. This has an influence on the range resolution, and the resolution cell in range can, depending on the TEC values, increase by a factor of 3 for a frequency of 400MHz [23]. The resulting pulse broadening is also a function of the used bandwidth. Due to changes of the pulse group velocity, the position of the image changes and undergoes a shift in range. This shift increases with the values of the TEC [23].

• Faraday rotation

In spaceborne applications, long wavelength imaging systems (like P–band systems) are strongly affected by Faraday rotation, an effect that arise due to the circular bi–refringent behaviour of the ionosphere caused by the earth magnetic field which results in different propagation constants for the two left– and righthanded polarized parts into which a wave can be split up. For a generally polarized wave the change of the ellipticity angle can be neglected, but not the rotation of the orientation angle. The amount of Faraday rotation depends on the Total Electron Density (TEC) profile, the Earth's magnetic field (increases with the inverse square of the radar frequency) and the elevation angle. Faraday rotation is also a function of time. For example the maximum likely Faraday rotation at a system operating at the frequency of 400MHz is 675^0 during the day and only 67^0 at night [30].

The Faraday rotation effect in VHF/UHF frequencies is quite strong and any attempt of polarimetric calibration of the collected data becomes very challenging. It is known [24] that for frequencies above 100MHz, the one–way Faraday rotation angle Ω is given by :

$$\Omega = K_F f^{-2} B_{propa}^{-} \int_{path} N_e ds \qquad (8)$$

Where f is the system frequency, B_{propa} is a weighted mean value of the magnetic field component along the propagation direction, N_e is the electron density, s is the path length, and K_F is a constant. The integral express the TEC value along the slanted ray path.

For the spaceborne P–band case, including Faraday rotation, the model of equation (7) which describe the systems effects becomes:

$$[O] = [R][F][T] + [N] \qquad (9)$$

where $[O]$ is the 2x2 observed scattering matrix, $[F]$ is the scattering matrix given by:

$$F = \Omega S \Omega \qquad (10)$$

With the Ω Faraday rotation matrix given by:

$$\Omega = \begin{pmatrix} \cos\Omega & \sin\Omega \\ -\sin\Omega & \cos\Omega \end{pmatrix} \qquad (11)$$

The sign of Ω is positive in the northern hemisphere in a right–handed coordinate system with $x=H$, $y=V$, and z toward the Earth [25]. $[R]$ and $[T]$ are 2x2 complex matrices describing amplitude and phase distortions in the receiver and transmit path respectively and $[N]$ is the system noise [25]. Like in the airborne case, the system calibration involves solving (9), using only the observed matrix $[O]$ and some knowledge of the scattering properties $[S]$, to obtain the distortion matrices $[R]$ and $[T]$ as well as the Faraday matrix.

The magnetic field can be assumed for practical reasons, to be both static and homogeneous over typical scenes and aperture formation types. However, spatial variability in B_{propa} occurs because the line–of–site of the radar with respect to the magnetic field direction changes as the radar moves. This is one of the main sources of azimuth defocusing effects as already mentioned. The value of the resulting Faraday variations $\Delta\Omega_m$ over the synthetic aperture radar length L at an altitude h is given for $L \ll h$ by [25] :

$$\left| \frac{\Delta\Omega_m}{\Omega} \right| \approx \frac{L}{h} \sin\varphi_0 \cos\psi_0 \qquad (12)$$

where φ and ψ are the angles between the aperture plane and the magnetic field direction respectively, as illustrated in Figure 7, with φ_0 and ψ_0 the corresponding mean values. For a relatively low SAR platform altitude of 600 km (as proposed for BioSAR [31]

$$\left| \Delta\Omega_m / \Omega \right| < 0.002L \quad \text{for all values of } \varphi_0 \text{ and } \psi_0.$$

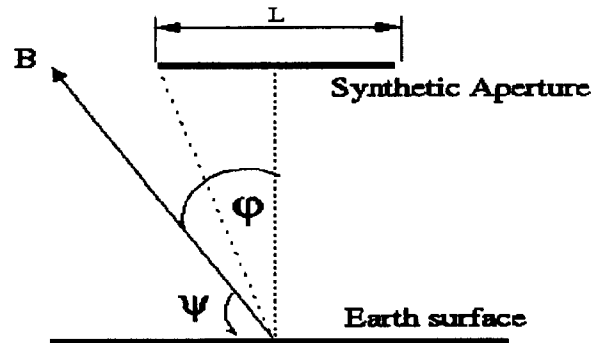The solution of (9) is quite complicate and it is under investigation.

Figure 7: *Imaging geometry of the imaging sensor and the magnetic field.*

Once the Faraday rotation has been measured the SAR system may need to adjust the plane of the

transmitted polarization to achieve the wanted polarization on the ground (Figure 7).

Freeman in [24] modeled the Faraday rotation in a spaceborne SAR backscatter case and presented a new approach for estimating the Ω, while overcoming also the problem of the modulo 2π errors. The proposed approach improves the numerical solutions offered by Gail [25] and the approach of Rosen [26] which uses ground based corner reflectors.

The idea of using the RFI signal from the terrestrial communication channels to the SAR system [30] as reference signals for measuring the Faraday rotation does not seem to be valid any more as the LO analysis proved that it is very likely to have interference tones for both polarization states (fully polarimetric).

In order to overcome the problems introduced to the signal due to Faraday rotation, a common approach for a spaceborne VHF/UHF SAR system design is to use circular polarised signals. A circular polarised signal is less sensitive to the Faraday rotation but at the same time is limiting the use of a spaceborne VHF/UHF SAR system for applications like the Biomass estimation [30].

Using this circular polarised signal configuration, Shteishleiger et al [28] proposed a new approach for compensating the ionospheric distortions using a two dimensional adaptive filter in the receiver for chirp compression where the reference phase function is matched with the received signal that has passed through the ionosphere (and not with the radiated chirp signal). The 2D-compensation algorithm has been tested with real airborne VHF/UHF SAR data where ionospheric distortions have been simulated, with quite promising results.

Nevertheless, in the recent years, DLR has gained a lot of experience in calibration of X-SAR, SIR-C and recently SRTM space shuttle missions, and several calibration techniques have been developed and successfully implemented [13],[14]. Since night-time P-band Faraday rotation is predicted to be comparable with L-band day-time Faraday rotation, similar calibration techniques (like in L-band) could be easily developed for operating a spaceborne P-band SAR even at linear polarisation at night-time [30].

- **RF Interferences in spaceborne P-band SAR**

As already analysed in details for the airborne P-band SAR system, RFI are a mutual problem when frequency bands are shared between different services. Hence, for the spaceborne P-band case two types of interference will be discussed.:

1. RFI from the terrestrial communication services to the SAR imaging sensor and
2. RFI from the P-band spaceborne sensor to the terrestrial communication services.

1. As already analysed in section 3.1 the interference caused by the large number of interference sources within the SAR's field of view, will degrade the data quality (examples of this effect is shown in Figures 2a and 2b). The same algorithms (notch filter and LMS

estimation and subtraction algorithm) developed for the airborne E-SAR P-band system can be applied without any difference and with the same results in a spaceborne P-band sensor. Especially the application of the LO channel mode of operation can offer almost real time RFI filtering [3],[4],[5]. Additionally in order to increase the acceptability of the system, it is attractive to operate during the night when the communication services are used less.

2. The spaceborne SAR illuminates a strip beneath and to one or both sides of the satellite. The strip can be between tens and hundreds of kilometres wide and can be thousands of kilometres long. The revisit time (the time between passes of the satellite over the same geographic area) is normally between 3 and 30 days. Hence, during the illumination time, a big number of terrestrial communication stations will be within the scanned area, but interference caused by the radar will be less than once per day.

The operation parameters of a common communication channel (Table 3) and the system specifications of the proposed spaceborne P-band BioSAR (Table 4) system was analysed in order to determine the interference effect from a P-band spaceborne SAR sensor to the terrestrial communication links.

BioSAR is a fully polarimetric spaceborne P-band system design proposed to ESA by a group of companies as described in [32]. The basic aim of the proposed system is the measuring of the geophysical parameters like biomass, flooding condition, and land cover class. Using the design parameters of tables 3 and 4 the peak radiated field strength on the surface of the Earth P_{BioSAR} due to the spaceborne sensor is given by [31] :

$$P_{BioSAR} = \frac{Peak\ Transmit\ Power}{R\ \beta_{BioSAR}\ W_{BioSAR}} \quad (13)$$

Where for $\beta = 7^0$ becomes 1.310^{-6} W/m² and for $\beta = 9^0$ 1.06 W/m²

Parameter	Symbol	Fixed Comm. Station	Mobile Comm
Transmit power	P_{COM}	100W	10W
Antenna Polarization		Vertical	Vertical
Antenna Gain (Horizontal)	G_{COM}	2dB	2dB
Antenna Gain (towards satellite)	$G_{COM-SAT}$	0dB	0dB
Receiver Noise Figure	F_{COM}	2(3 dB)	2(3 dB)
Transmit Bandwidth	B_{COM}	10kHz	10kHz
Transmit condition		continuously	continuously

Table 3. *Operational parameters of a common fixed and mobile terrestrial communication service.*

This calculated energy is spread over the whole bandwidth of the transmitted chirp pulse. For this reason, the effective strength of the received field within the bandwidth of the terrestrial communication system must be also calculated. Using the parameters of Table 3 we get [31] :

$$P_{BioSAR} \cdot \frac{B_{COM}}{B_{BioSAR}} = 1.6 \quad \text{or} \quad 1.3 \cdot 10^{-9} W/m^2 \qquad (14)$$

In order to compare the strength of this interference signal with the corresponding strength of communication signal, the field strength of a fixed and a mobile communication transmitter for a distance r=10km, has been calculated.

$$P_{comm\,field\,strength} = \frac{P_{COM} \cdot G_{COM}}{4\,\pi \cdot r^2} \qquad (15)$$

at a mobile receiver we get : 1.3 10^{-7} W/m^2 and at a fixed station: 1.3 10^{-8} W/m^2.

Comparing these values with (14) we see that the SAR signal is for a mobile station two order of magnitude below the communication signal level and one order for fixed station.

But in order to estimate the interference generation to the communication channels, the sensitivity of the communication receivers (the limiting field strength due to noise), must be calculated.

$$\frac{Noise\,Density}{Effective\,Antenna\,Aperture} = \frac{B_{COM} \cdot (F_{COM} - 1)\,290 \cdot k}{G_{COM} \cdot \lambda^2/4\,\pi} W/m^2$$

$$(16)$$

Where k is the Boltzman's constant, and λ is the systems wavelength. For BioSAR with λ=0.689m (16) becomes equal with $8,38 \cdot 10^{-16}$ W/m^2. The resulting sensitivity is much smaller than the direct path strength of the transmitted SAR signal (as expected to be) [31].

BioSAR System Specifications		
Parameter	Symbol	Value
Spacecraft Altitude above Nadir	R	600 Km
Swath width	W $_{BioSAR}$	50 Km
Incidence angle at mid swath	φ	23 ^{0}
Center frequency	F $_{BioSAR}$	435 Mhz
Chirp pulse bandwidth	B $_{BioSAR}$	8 Mhz
Antenna beamwidth (azimuth)	β $_{BioSAR}$	7 ^{0} or 9^0
Peak transmit power	P $_{BioSAR}$	50 W

Table 4. Basic BioSAR operating parameters.

Even though, the SAR signal has an average power comparable with the strong communication signals, and therefore will cause interference to the users, it is not so strong that the terrestrial communication links will be overloaded. We must also note that the reliability required by the mobile phone links is less than 10 minutes per year and therefore the disturbance caused by a spaceborne P–band SAR seem to be acceptable [31],[33].

• **Frequency allocation**

The final investigation subject of our spaceborne P–band SAR analysis is the problem of the frequency allocation. We let this problem last as it is more close to a politic decision and less a scientific/technological problem.

The frequency allocations for spaceborne applications are derived from the International Telecommunication Union (ITU). Unfortunately no primary or secondary allocation for active spaceborne sensors below 1GHz exists. The range up to 406 Mhz includes meteorological aids which can include weather radars with high transmit power and antennas pointing skywards. The band above 470 MHz is allocated to broadcasting, mainly TV stations with high continuos transmit power [31]. In between the band is allocated by fixed and mobile communication stations. As these services mainly use low power and antennas pointing horizontally, this band is mainly considered for the proposed P–band spaceborne SAR sensors (BioSAR). As already mentioned this band has no provision for operation by spaceborne SAR sensors, but as analyzed above the mutual interferences are tolerable. Hence, it shall not be too difficult to obtain permissions from the regulations authorities.

5. CONCLUSIONS

Low frequency fully polarimetric, interferometric Synthetic Aperture Radar has proven to be a very powerful method for underground and obscured object detection as well as for geophysical parameter estimation. In this paper the possibility of a spaceborne P–band SAR system, based on the experience gained from the analysis of the experimental airborne P–band SAR system of DLR is presented. Concepts like the low frequency SAR hardware design configuration, the algorithms used for polarimetric and radiometric calibration and finally RFI suppression techniques concerning the airborne P–band case have been discussed and analyzed. Extension of the advantageous low frequency remote sensing technique to a global scale by a spaceborne P–bands SAR sensor is addressed. For this case the several problems that ionosphere introduces to the system like the reduced azimuth and range resolution, the displacement of the imaged scene, the Faraday rotation, the necessity of accurate TEC measurement and the frequency allocation, have been analyzed and possible solutions are given.

The Radio Frequency Interference problem introduced from the terrestrial communication channels to the spaceborne sensor and vice versa have been analyzed. Especially, for the second case of RFI generation to the terrestrial communication channels, the design specifications of the proposed BioSAR sensor have been used and the analysis proved that the possible disturbance caused by a spaceborne system to a communication services seem to be acceptable.

6. ACKNOWLEDGMENTS

7. REFERENCES

[1] R. Horn : "The DLR Airborne SAR Project E–SAR."Proceedings of IGARSS'96 Lincoln, Nebraska USA. pp. 1624–1626, 1996.

[2] R. Scheiber, A. Ulbricht, A. Reigber, K.P Papathanassiou:"Airborne Interferometric SAR Activities in DLR". RTO Meeting, High Resolution Radar Techniques. Granada, Spain March 1999.

[3] A. Potsis, A. Reigber, T. Sutor and K.P Papathanasiou:"A phase Preserving Method for RF Interference Suppression in P–Band Synthetic Aperture Radar Interferometric Data." Proceedings of IGARSS'99 Hamburg, pp. 2655–2658, 1999.

[4] A.Potsis, S. Buckreuss, R. Horn and N. Ouzunoglu : "P–Band Interference Study Using Information From The New E–SAR Listen Only Channel Mode Of Operation". Proceedings of USAR2000,Munich/ Germany, May 2000, pp 855–857.

[5] S. Buckreuss and T. Sutor 1998 :"Suppression of interfernces in P–band SAR data". International Radar Symposium, DGON Munich, Germany.

[6] Ritcard T. Lord and Michael R. Inggs 1998: "Approaches for RF Interference Suppression for VHF/UHF Synthetic Aperture Radar." Proceedings IEEE South African Symposium on Communication and Signal Processing, COMSIG'98 , Cape Town, South Africa.

[7] G. Cazzaniga, A.Monti Guarmieri 1996: "Removing interferences from P–Band aeroplane SAR data." Proceedings of IGARSS'96 Lincoln, Nebraska USA Vol.III. pp .460–463

[8]A.Potsis, B.Gabler, R.Horn, K. Papathanassiou and A.Reigber: "End–To–End calibration Of Polarimetric P–Band Data of DLR Experimental SAR (E–SAR)" Proceedings of USAR2000,Munich/ Germany, May 2000, pp 855–857.

[9] L.M.H Ulander May: 'Radar remote sensing for sea ice: Measurment and theory', Chalmers University of Technology, Goteborg, Sweden, Tech. report 212, 1991.

[10] L.M.H Ulander: 'Accuracy of using point targets for SAR calibration', IEEE Trans. Aerospace Electon. Syst. Vol. 27, No.I, pp. 139–148, 1991.

[11] K.P. Papathanasiou, M. Zink: Polarimetric Calibration Of the Airborne Experimental SAR System Of DLR. Proceedings Of European Conference On Synthetic Aperture Radar, Proceedings of EUSAR'98, Friedrichshafen, Germany, 1998.

[12] A. Freeman," SAR Calibration: An overview", IEEE Transactions On Geoscience and Remote Sensing, Vol 30, Nov 1992, pp 531–539.

[13]M. Zink, R. Bamler: " X–SAR Radiometric Calibration and Data Quality", IEEE Transactions On Geoscience and Remote Sensing, Vol 33, Jul. 1995, pp 840–847.

[14] M. Zink, D. Geudtner: "First Results from the Calibration of the interferometric X–SAR system of SRTM", Proceedings of EUSAR'2000, Munich, Germany, 2000.

[15] S. Quegan, J. Lamont:" Ionospheric and Tropospheric effects on synthetic aperture radar performance", International Journal For Remote Sensing, no 71986, pp. 525–539.

[16] Daniell, R.E., Brown, L.D., Anderson, D.N., Fox, M.W., Doherty, PH., Decker, D.T., Sojka, J.J., Schunk. R.W.," Parameterized ionospheric model: A global ionospheric parameterization based on first principle models", Radio Sci, vol 30, 1499–1510 (1995)

[17]Davis, K., "Ionospheric Radio Waves", Blaisdell Publishing Comp., Waltham, Massachusetts, (1969)

[18]Ho, C.M., Wilson, B.D., Mannucci, A.J., Lindqwister, U.J., Yuan, D.N., "A comparative Study of ionospheric total electron content measurements using global ionospheric maps of GPS, TOPEX radar, and the Bent model", Radio Sci., vol 32, no 4, 1499–1512, July–Aug (1997)

[19]Ho, C.M., Mannucci, A.J., Sparks, L., Pi, X., Lindqwister, U.J., Wilson, B.D., Iijima, B.A, Reyes, M.J., "Ionospheric total electron content perturbations monitored by the GPS global network during two northern hemisphere winter storms", J. Geophys. Res., vol 103, no A11, 26409–26420, Nov. (1998)

[20] Iijima, B., Harris, I.L., Ho, C.M., Lindqwister, U.J., Mannucci, A.J., Pi, X., Reyes, M.J., Sparks, L., Wilson, B.D., "Automated daily process for global ionospheric total electron content maps and satellite ocean altimeter ionospheric calibration based on Global Positioning Systems data" , J. Atmos. Solar–Terrestrial Physics, vol 61, 1205–1218 (1999)

[21] Mannucci, A.J., Wilson, B.D., Edwards, C.D., "A new method for monitoring the earth's ionospheric total electron content using GPS global network", Proc.Sixth Int. Technical Meeting of the Satellite

Division of of the Inst. of Navigation, Inst. Navig. Alexandria, Va., 1323–1333 (1993)

[22]Pi, X., Mannucci, A.J., U.J.Lindqwister, Ho, C.M., *"Monitoring of Global Ionospheric Irregularities using the Worldwide GPS Network"*, Geophys. Res. Letters, vol. 24, no. 18, 2283–2286, Sept.15 (1997)

[23] A. Ishimaru, Y. Kuga, J.Liu, Y. Kim, A. Freeman: *"Ionospheric effects on synthetic aperture radar at 100 MHz to 2GHz"*, Radio Science, Vol. 34, no 1,Jan–Feb 1999,pp.257–268.

[24]*A. Freeman, S. Saatchi: "The Effects of Faraday Rotation on Backscatter Signatures in SAR Image Data"*, SPIE, vol 3120, 1997 pp37–44

[25] W.B Gail: *"Effect of Faraday Rotation on Polarimetric SAR"*, IEEE Transactions On Geoscience and Remote Sensing, Vol 34, no 1 January 1996, pp 301–307.

[26]P. Rosen, *"Faraday Rotation"*, JPL memorandum.

[27] *D.M Vine, M. Kao: "Effects of Faraday Rotation on Microwave Remote Sensing from Space at L–band"* Proceedings of IGARSS'97 AUGUST 1997. pp 377–379.

[28] *V. Steinshleiger, A. Dzenkevich, V. Manakov, L. Melnikov, G. Misezhnikov:" Quantative Characteristics of Two–Dimensional Adaptive Compensation for Ionoshperic destructive Influence on VHF Spaceborne SAR Resolution"*. Proceedings of EUSAR2000,Munich/ Germany, May 2000, pp 419–422.

[29] V. Blinov: *"Preasence Refinement of Ionoshperic Parameters For Function Securing Of Spaceborne VHS SAR"*, Proceedings of USAR2000,Munich/Germany, May 2000, pp 407–410E.J. Rignot, R.

[30]R. Zimmermann, J. Van–Zyl:*" Spaceborne Applications of P–band Imaging Radars for Measuring Forest Biomass"* EEE Transactions On Geoscience and Remote Sensing, Vol 33, no 5, 1995, pp 1162–1169.

[31] M. Chandra, D. Hounam:*" Feasibility of a Spaceborne P–band SAR for Land Surface Imaging"*, Proceedings of EUSAR'98, Friedrichshafen, Germany, 1998.

[32]F.M. Seifert, P. Snoeij: *" Biomass Mapping Satellite System (BioSAR)"* Proceedings of EUSAR2000, Munich/ Germany, May 2000, pp 81–84.

[33]S. Buckreuss, M. Chandra, D. Hounam:" Low Frequency SAR Criticalities", Study for ESA–ESTEC 1997.